Journal of Alloys and Compounds, Volume 822, May 2020, Article number 153751
DOI: 10.1016/j.jallcom.2020.153751

Facile synthesis of TiN nanocrystals/graphene hybrid to chemically suppress the shuttle effect for lithium-sulfur batteries

J. Tu, H Li, T. Lan, SZ. Zeng, J. Zou, Q. Zhang, X. Zeng

Abstract

Herein, we present a microwave reduction strategy for the synthesis of reduced-graphene-oxide (rGO) supported TiN nanoparticle hybrid (TiN/rGO) under N_2 atmosphere. The method involves GO reduction, metal oxide reduction and nitridation reaction in one single step. Due to TiN high conductivity and good interfacial affinity between it and lithium polysulfides (LiPSs), the prepared TiN/rGO-Sulfur (TiN/rGO-S) cathodes demonstrate rapid charge transfer, lower polarization, faster surface redox reaction kinetic and enhanced stability cycling performance than rGO-Sulfur (rGO-S) and TiO_2/rGO-Sulfur (TiO_2/rGO-S) cathodes. The initial capacity reaches 1197.6 mA h g^{-1} with a reversible capacity of 888.7 mA h g^{-1} being retained after 150 cycles at 0.1 C.

Keywords

Lithium-sulfur batteries, Shuttle effect, Titanium nitride, Microwave reduction, Chemisorption

1. Introduction

To date, the electrical energy storage appliances ranging from portable electronics, clean-energy vehicles to the intermittent renewable energy involving solar and wind energy in the modern smart electrical grid have made enormous strides, however, the high demand for such technological advancements is ever present [[1], [2], [3]]. Thus, the development of advanced battery systems with high power density, high capacity, low cost and long cycle life is desirable [[4], [5], [6]]. However, the energy density of current rechargeable lithium-ion batteries (LIBs) using electrodes based on Li^+ insertion chemistry is approaching its formidable limitation, making it exceedingly difficult to satisfy this rapidly growing area [[7], [8], [9]].

Published by Elsevier. This is the Author Accepted Manuscript issued with: Creative Commons Attribution Non-Commercial No Derivatives License (CC:BY:NC:ND 4.0).
The final published version (version of record) is available online at DOI: 10.1016/j.jallcom.2020.153751. Please refer to any applicable publisher terms of use.

Over the past few years, rechargeable lithium-sulfur batteries (LSBs) are regarded as the most commercial potential energy storage system for the next-generation, due to its large theoretical specific capacity (1675 mAh g^{-1}) and extraordinary energy density (2600 Wh kg^{-1}), which is much higher than the corresponding values of extant LIBs [10]. Additionally, elemental sulfur possesses additional superiorities as a cathode material owing to its readily availability, relatively low-price, and non-poisonous [11].

Nonetheless, the practicality of reliable LSBs is still impeded by two main technical challenges. Firstly, the poor conductivity of sulfur and its discharging products (e.g. Li_2S and Li_2S_2) lead to low utilization of active material [12]. Secondly, the easy dissolution and transportation of lithium polysulfide intermediates (LiPSs, Li_2S_x, x goes between 2 and 8) produced at the charging/discharging processes trigger the so-called 'shuttle effect', which can result in rapid capacity degradation and low coulombic efficiency [13]. Therefore, the electronic conductivity ability and reduction of the 'shuttle effect' are issues that urgently need to be rectified for the development of Li–S batteries [14].

Currently, extensive explorations have been conducted to tackle these obstacles of LSBs. One of the effective strategy is to make a sulfur composite with carbon-based materials because of its high-conductivity, great specific surface area, low cost and diverse morphologies, such as hollow carbon nanospheres [15,16], carbon nanotubes [17,18], carbon nanobelts [19], activated carbon and graphene [20,21]. Among them, two-dimensional (2D) graphene nanosheets are considered to possess an exceptional matrix material for sulfur nanoparticles, owing to superb electronic conductivity, ultrathin thickness, structural flexibility, chemical stability and high surface-to-volume ratio. Numerous reports have examined the fabrication of graphene-sulfur hybrid as cathode materials for LSBs. However, these studies show that pure graphene as a sulfur host material is only advantageous to ameliorate the terrible electronic transmission capability of elemental sulfur but has little effect on restricting the migration of LiPSs because

of the non-polarity of carbon atom [22]. Although the dissolution and shuttle effects of LiPSs have been restrained to some extent, the correlated capacity still suffers significant decay upon long-term cycling.

Recent reports have shown that the cycle stability of carbonaceous based electrode materials is greatly enhanced after modification with polar metallic oxide nanoparticles such as SiO_2 [23,24], SnO_2 [25,26], TiO_2 [27], Ti_4O_7 [28,29] and MnO_2 [30], which have been employed as effective polysulfide adsorbents owing to the strong chemical binding to LiPSs. Nevertheless, most aforementioned metal oxides are semiconductors or insulators, which seriously obstruct electron transmission and conversion of soluble LiPSs into insoluble products, promoting lower sulfur utilization and inferior rate performance. Therefore, it is imperative to introduce certain bi-functional materials that combine inherent metallic conductivity and strong adsorption capability to LiPSs into the sulfur electrode to remove these blockages.

Compared to metal oxide, transition-metal carbides or nitrides (TiC [31], WC [32], MoC [33], TiN [34], WN [35], VN [36], ZrN [37], NbN [37], etc.), possessing high conductivity, chemical stability, a polar surface and electrochemical catalytic activities, have recently become of interest. Goodenough's group were the first to present a novel matrix material of TiN with mesoporous morphology, which was used as the conductive agent and adsorbent for LiPSs and prepared by a solid-solid thermal process under NH_3 atmosphere [38]. Fan et al. designed and fabricated a MoN supported graphene (MoN/G) inter-layer via an annealing process using NH_3 as the reducing agent and nitrogen sources at 850 °C for 6 h. The obtained MoN/G inter-layer displayed strong anchoring capacity for LiPSs as well as accelerated Li_2S decomposition ability [39]. Zhang et al. synthesized a Ti_3C_2 MXene conductive paper for sulfur host materials, which show good mechanical stability, excellent conductivity and unique chemical adsorption of LiPSs. Ti_3C_2 MXene was prepared by exfoliation of Ti_3AlC_2 powders in the HCl and LiF mixed solution (HCl 6 M 10 mL, LiF 0.666 g). Furthermore, the Ti_3AlC_2 powders were synthesized

by mixing TiC and Ti_2AlC particles through ball milling for 18 h, and then heated at 1350 °C for 2 h [40]. These studies clearly show that the robust bonding between high conductive transition-metal nitrides or carbides and LiPSs can greatly mitigate the shuttle effect. Nevertheless, the preparation technique of metal carbides or nitrides usually requires rigorous synthesis conditions, such as high temperature, corrosive acid and toxic gases reactants, leading to excessive energy consumption, environment damage and low-efficiency, making unsuitable for large-scale industrial production.

Herein, we introduce a microwave-assisted reduction strategy for the preparation of layered reduced oxide graphene sheets supported TiN nano-particles composite (TiN/rGO) under N_2 atmosphere. TiO_2 nano-particles hybridized with graphene oxide (TiO_2/GO) were first prepared by a facile solvent method using tetra-*n*-butyl titanate (TBOT) as the titanium source at room temperature. These composites were completely transformed into TiN/rGO within 10 min by microwave heating reduction. The as-prepared TiN/rGO hybrid served as the sulfur host material, exhibiting several advantages: the lamellar graphene structure affords channels that allow lithium ions and electrons to be freely transferred; the well-distributed TiN nanoparticles anchored on graphene sheets act as an adsorbent, trapping LiPSs owing to enhanced chemical interactions, which alleviates the shuttling effect; the metallic TiN forms an excellent interface with LiPSs improving reductive catalyization of sulfur and oxidation of Li_2S.

2. Experimental

2.1. Synthesis of anatase TiO_2/rGO

The TiO_2/GO hybrid was synthesized by a facile in situ solvent method. Typically, 0.2 g original commercial graphene oxide powder (NanJing JI Cang Nano Technology Co. Ltd. Model: JCGO-95-1-2.6) was dispersed in 200 mL ethanol solution in a sealed serum bottle

under ultrasonic vibration for 12 h. Then, the solution of 360 μL TBOT in 50 mL ethanol was added dropwise into the above mixture with continuously stirring. The hydrolysis reaction was initiated upon exposure to air at 26 °C for half a day. The resulting black product was filtered, and then the filtered TiO_2/GO film was dried at 80 °C overnight. Finally, the anatase TiO_2/rGO composite was obtained by cutting the film into pieces, which was transferred to the tube furnace, followed by annealment at 600 °C for 2 h. For comparison, the control group of rGO was prepared under the same conditions.

2.2. Synthesis of TiN/rGO by microwave

At first, the as-prepared dry TiO_2/GO pieces were ground into a fine powder and loaded into a SiC coated graphite tube. Subsequently, the tube was placed in the microwave reactor (NanJing JieQuan Microwave Equipment Co. Ltd. Classic NJZ4-3 Microwave Oven). The reaction was rapidly heated to 1200 °C and held for 10 min, then cooled to room temperature under N_2 atmosphere.

2.3. Synthesis of host material and sulfur composites

The TiN/rGO-Sulfur (TiN/rGO-S) hybrid was synthesized via the classical melt-infiltration method: the prepared TiN/rGO powder was mixed uniformly with the commercial sublimed sulfur (Shanghai Aladdin Biochemical Technology Co., Ltd. Model: S106611) in a mass ratio of 40:60, and heated the mixture to 155 °C for 12 h. For comparison, TiO_2/rGO-Sulfur (TiO_2/rGO-S) and rGO-Sulfur (rGO-S) composites with equal sulfur content were synthesized under the same conditions.

2.4. Characterization of the samples

The morphologies and element distributions of rGO, TiO_2/GO, TiN/rGO, and their sulfur-containing composites were confirmed using a scanning electron microscope (SEM, Hitachi SU-70) and transmission electron microscope (TEM, Tecnai G2 F20 S-TWIN, FEI, and 200 kV). The crystallographic structure of the samples were characterized by X-ray diffraction

(XRD, Rigaku SmartLab, 40 kV and 200 mA), and the data was collected from 2θ = 10–80°. The Raman spectra of the samples were measured by a Raman Microscope (RENISHAW invia, λ = 514.5 nm). The sulfur content of the hybrids was identified by thermogravimetric analysis (Discovery TGA-55). The chemical interaction between the TiN/rGO and LiPSs was characterized by X-ray photoelectron spectroscopy (XPS, Microlab350). The specific surface area of the composites was confirmed by nitrogen adsorption-desorption analysis (Micromeritics Co. ASAP 2020).

2.5. Cell assembly and electrochemical test

In the case of cathode preparation, the as-prepared sulfur composites were mixed with carbon black and LA133 aqueous binder in a mass ratio of 80:15:5. The slurry was prepared using adequate ethylalcohol and *N*-methyl-2-pyrrolidone (NMP) as a solvent, then coated uniformly on aluminum foil with a scraping plate and dried at 60 °C in vacuum for half a day. Then, the aluminum foil was stamped into circular discs with a typical diameter of 16 mm. In order to ensure consistent sulfur content, the control group TiO_2/rGO-S and rGO-S were synthesized under the same processing conditions. All electrochemical tests were conducted on standard CR2016 type coin cells with the micro-porous polypropylene membrane as separators (Celgard2400, America). The entire assembly processes were conducted in a glove box filled with highly pure argon gas (H_2O < 0.10 ppm; O_2 < 0.1 ppm). The charge-discharge test was performed at a voltage window between 1.8 and 3.0 V (vs. Li/Li^+) on an automatic batteries test instrument (Land CT 2001A, model 5 V-10 mA). The capacities of the assembled button cells were calculated by the mass of sulfur (1C = 1670 mA g^{-1}). The sulfur loading of the sulfur electrode in Fig. 5a–e is 1.2 mg cm^{-2}, and the electrolyte/sulfur ratio is 1 mg sulfur: 15 μL electrolyte. The corresponding electrochemical properties include cyclic voltammetry (CV) and electrochemical impedance spectra (EIS) of the cells were tested by CHI660D.

3. Results and discussion

The preparation of TiN/rGO-S and TiO_2/rGO-S composite is outlined in Fig. 1. A series of different ratio of TiN and rGO were perpared by mixing 0.2 g GO with 0, 180, 360, and 540 μL tetrabutyl titanate (TBOT). The weight ratio of rGO and TiN was determined by TGA under O_2 atmosphere (Fig. S1a). The weight ratio of rGO (W_{rGO}) in TiN/rGO was calculated by W_{rGO} - (100% - W_{rGO}) · 29% = $W_{\text{Mass Loss}}$. The mass of TiN increases by 29% upon conversion to TiO_2 during the air heating process. Therefore, rGO contents in TiN/rGO was prepared by mixing 0.2 g GO with 0, 180, 360, and 540 μL TBOT are 100, 84.71, 62.98, and 48.92 wt%, respectively. The corresponding TiN contents are 0, 15.29, 37.02, and 51.08 wt%, respectively. The rate capabilities of the four samples were investigated by discharging-charging mode at a range of discharging rates from 0.1 to 2 C for each 10 cycles. As shown in Fig. S1b, the discharging capacity of TiN/rGO-S electrode increases with increasing TiN content from 0 to 37.02 wt%. However, the discharging capacity reduced when the TiN contents further increased to 51.08 wt%. Thus, the mixture ratio of 0.2 g GO with 360 μL TBOT was selected for further studies. After the process of microwave-heating, the amorphous TiO_2/GO hybrid (Fig. S2) was quickly converted into TiN/rGO nanocomposite in 10 min. As shown in Fig. 2e and f, the SEM images show that the TiN nano-crystalline are well-distributed and evenly anchored on the rGO sheets surface. The control group anatase TiO_2/rGO hybrid was prepared by annealing the amorphous TiO_2/GO composite at 600 °C for 2 h under N_2 atmosphere. As shown in Fig. 2c and d, beside the smaller particle size, the morphology of TiO_2/rGO is similar to the TiN/rGO. TGA analysis (Fig. S3) suggests that TiO_2 content of TiO_2/rGO hybrid is 38.73 wt%. The other control group rGO was achieved by reduction of GO under the same heating conditions. The electrical conductivity of all samples (Fig. S4) was measured by a four-probe resistivity measurement system. Unlike the curly and wrinkled surface of TiO_2/rGO and TiN/rGO composites, the original rGO nano-sheets are thin and flat (Fig. 2a and b). Notably, the layered structure of the samples is largely preserved.

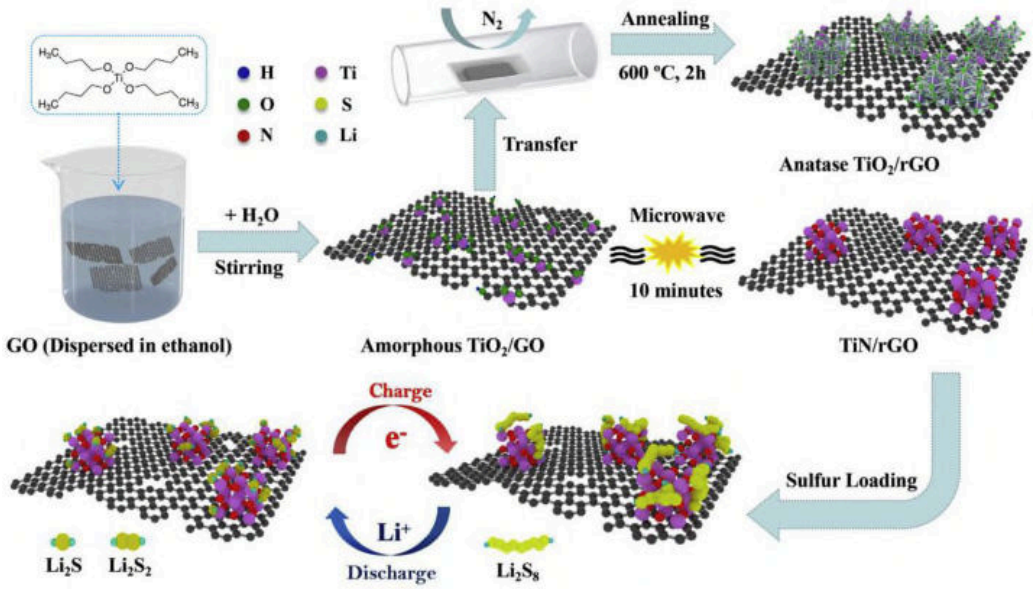


Fig. 1. A schematic illustration for the preparation of TiN/rGO-S and TiO_2/rGO-S.

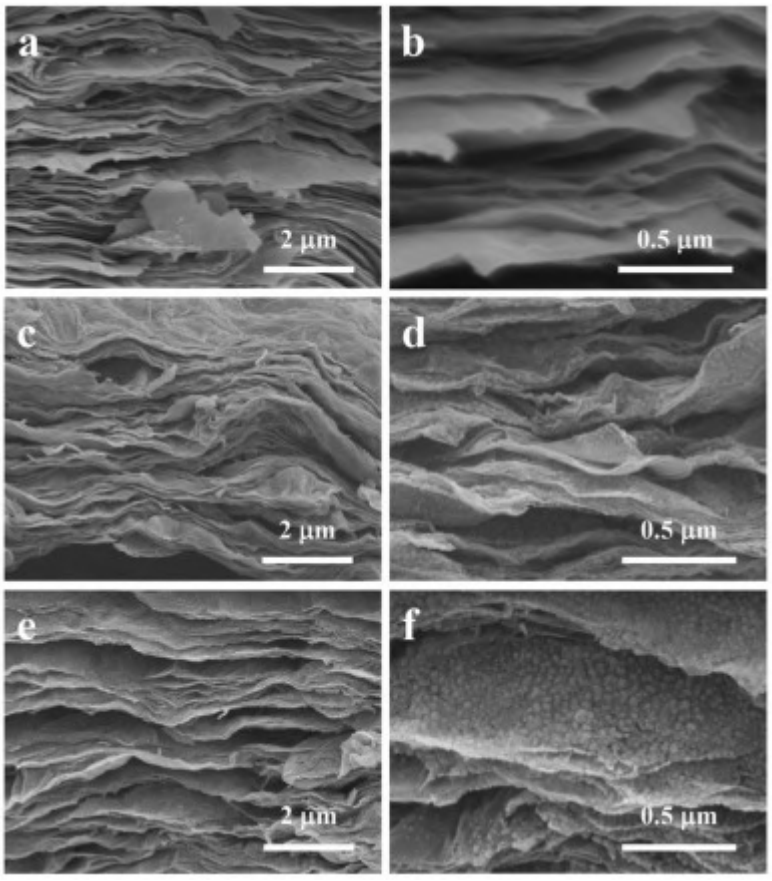


Fig. 2. (a,b) SEM images of pure graphene sheets; (c,d) SEM images of. anatase TiO_2/rGO; (e,f) SEM images of TiN/rGO.

The structure and morphology of TiO_2/rGO and TiN/rGO composites were further analyzed by TEM. As shown in Fig. 3a and b, TiO_2 nanoparticles with size distribution of 5–20 nm are evenly anchored on the surface of graphene, and no serious agglomeration is observed. The high-resolution TEM (HRTEM) images (Fig. 3c) display clear lattice fringes with values of ca. 0.242 and 0.351 nm, corresponding to the d_{103}-and d_{101}-spacing of anatase TiO_2, respectively [41]. The Fig. 3d and e shows that the size of crystal grain grows to 10–50 nm after the microwave heating process. The spacing of the diffraction lattice fringe displayed in Fig. 3f are ca. 0.212 nm, which is consistent with the d_{200}-spacing of TiN. The enhanced bonding between TiO_2 and rGO nanosheets may benefit from a great quantity of oxygen-containing function groups on the surface of precursor GO. High cohesion between the amorphous TiO_2 and GO can also facilitate the transformation of amorphous TiO_2/GO to TiN/rGO composite under microwave reduction.

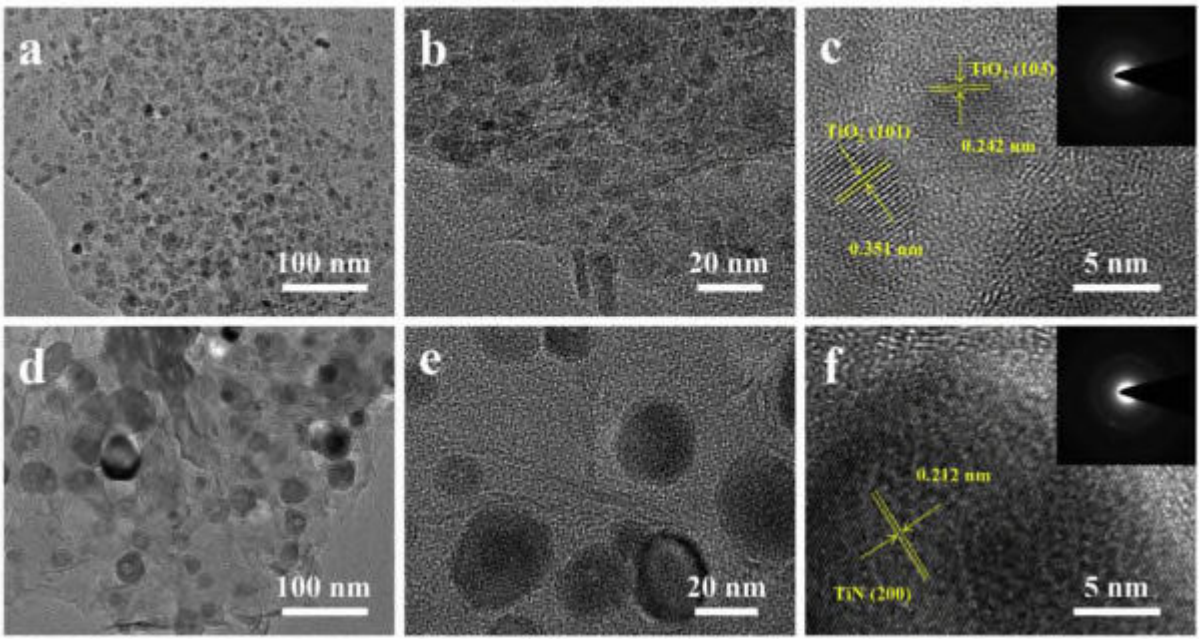


Fig. 3. (a–c) low magnification and high resolution TEM of the anatase TiO_2/rGO; (d–f) low magnification and high resolution TEM of the TiN/rGO.

The crystal structure of commercial GO, as-prepared rGO, TiO_2/rGO and TiN/rGO composite was confirmed through XRD. Fig. 4a shows the XRD patterns of the commercial GO nanosheets, an intensive diffraction peak appears at approx. 11° corresponding to the (001) diffraction of GO. A peak shift is observed toward the high angle side (ca. 26°) after microwave reduction, which is due to the (002) diffraction of rGO [42]. The typical peaks located at 36.65°, 42.57°, 61.78°, 74.02° and 77.91° in the XRD patterns are assigned to the (111), (200), (220), (311), and (222) planes of standard TiN (PDF # 87–0628), which indicates that the TiO_2/GO precursor is completely converted into TiN/rGO in high purity and crystallization [43,44]. The phase of TiO_2/rGO was also confirmed by XRD, with all diffraction peaks being consistent with anatase TiO_2 (PDF # 73–1764). Meanwhile, the diffraction of rGO is detected in the TiO_2/rGO and TiN/rGO composites, indicating that TiN and TiO_2 nanoparticles are closely integrated with rGO.

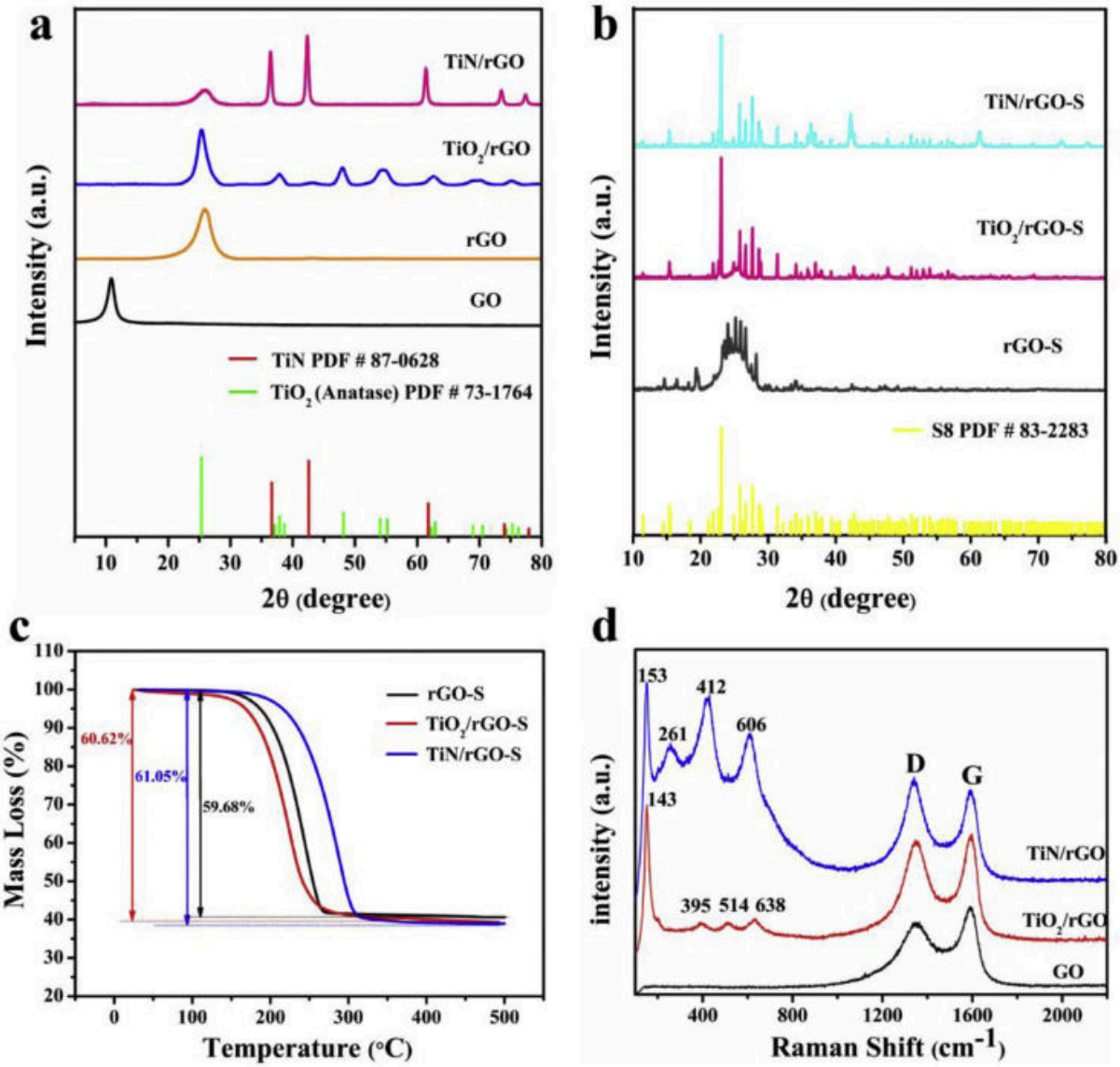


Fig. 4. (a) XRD pattern of GO, rGO, TiO_2/rGO and TiN/rGO, green and red drop lines correspond to anatase TiO_2 (PDF # 73–1764) and TiN (PDF # 87–0628); (b) XRD pattern of rGO-S, TiO_2/rGO-S and TiN/rGO-S, yellow drop lines correspond to sulfur (PDF # 83–2283); (c) TG curves of rGO-S, TiO_2/rGO-S and TiN/rGO-S; (d) Raman spectra of GO, TiO_2/rGO and TiN/rGO.

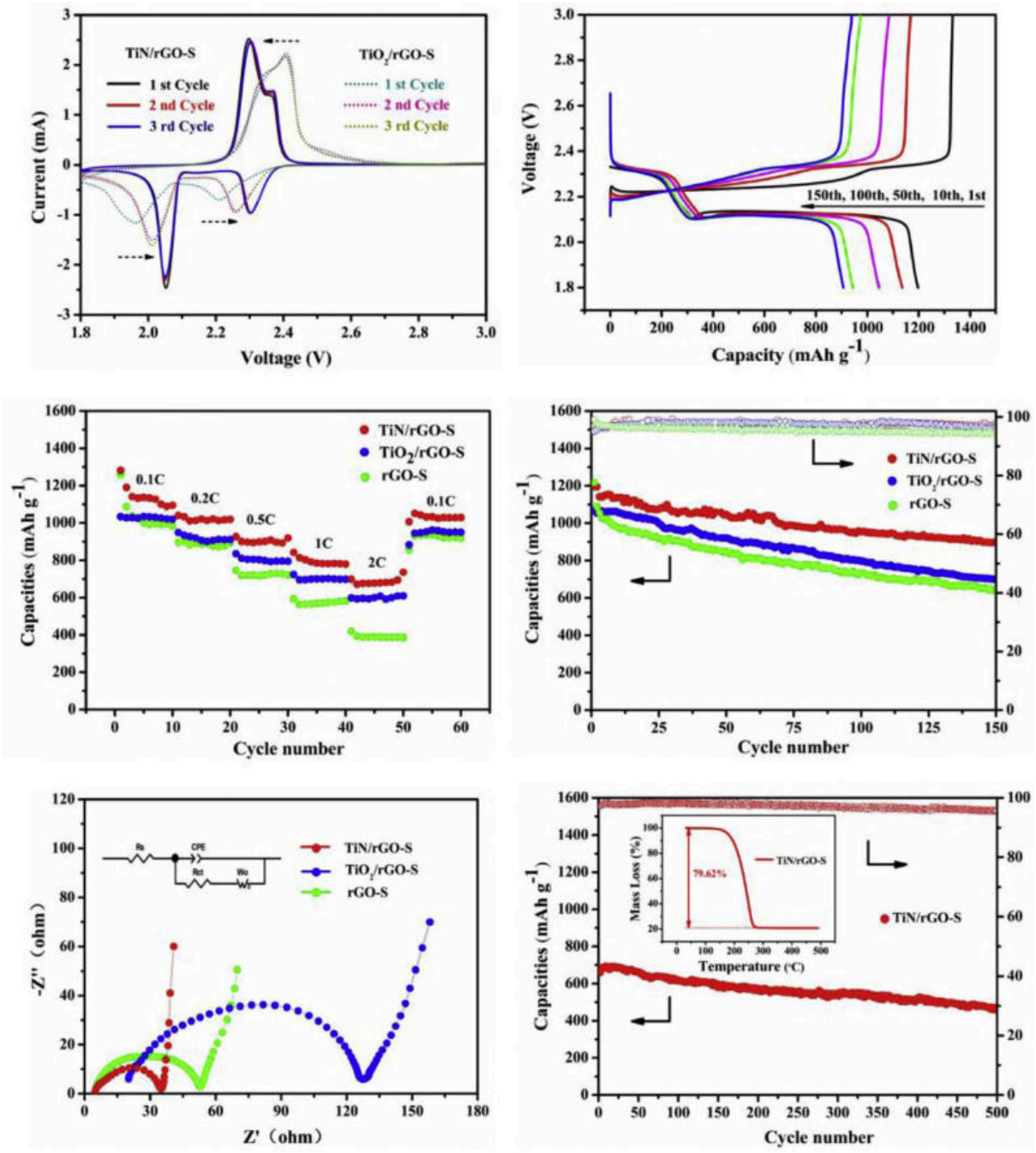


Fig. 5. Electrochemical performance. (a) CV profiles of TiO_2/rGO-S and TiN/rGO-S cathodes; (b) charge-discharge profiles of TiN/rGO-S cathode over different cycles at a current rate of 0.1C; (c) rate capacity, (d) cycling performance at 0.1C and (e) EIS spectra of rGO-S, TiO_2/rGO-S and TiN/rGO-S cathodes before cycling; (f) cycling performance of TiN/rGO-S cathode (with the sulfur content of 79.62% wt.) at a current rate of 1C.

The Raman spectra of pure GO, TiO_2/rGO and TiN/rGO hybrids are depicted in Fig. 4d. In the case of TiO_2/rGO composite, a strong Raman scattering peak is observed at 143 cm^{-1} due to

E_g vibration modes of anatase. Other peaks observed at approx. 385, 514, and 638 cm^{-1}, which are related to the typical vibrational modes of anatase [45]. Furthermore, four peaks at approx. 153, 261, 412, and 606 cm^{-1} are ascribed to TiN [46]. Notably, all samples exhibit a pair of adjacent intensive peaks at approx. 1350 and 1600 cm^{-1}, which correspond to the D- and G-band of GO and rGO, respectively. The D (disorder and defects) band commonly corresponds to the *k*-point phono on A_{1g} symmetry, and G (graphitic) band is ascribed to the in-plane stretching motion of symmetrical sp^2 C–C bond [47]. Accordingly, the TiN/rGO sample occupies the highest I_D/I_G intensity ratios (1.07), followed by TiO_2/rGO (0.97) and pure GO (0.85). Therefore, TiN doped graphene contains more defects than TiO_2 doped graphene and untreated GO, due to decomposition of the abundant oxygen-containing groups of the GO during the microwave reduction process. Fang et al. investigated the interaction between Li and defective graphene via first-principles calculations [48]. Results of this study demonstrate that the presence of vacancy defects can enhance the adsorption energy of Li in the region near the defect, because Li atom is easier to adsorb on the hollow site. Previous studies have also shown that the vacancy defects can physically accommodate the active materials sulfur and LiPSs and facilitate electrolyte infiltration [49]. On the other hand, the defects in the TiN/rGO composite, such as sp3 carbon and vacancy holes, can affect its conductivity to some extent. Therefore, the electrical conductivity of TiO_2/rGO, TiN/rGO, rGO (prepared in a tube furnace at 600 °C), and rGO (prepared in a microwave reactor at 1200 °C) were measured using the 4-point probes resistivity measurement system. As shown in Fig. S4, the different reduction processes have little influence on the electrical conductivity of rGO. Thus, we can assume that the defects in TiO_2/rGO and TiN/rGO have little impact on their electrical conductivity. Moreover, reports have shown that graphene's defects can facilitate the heteroatoms doping, which in turn contributes to improved conductivity [49].

Eq. (1) briefly describes the transformation process from amorphous TiO_2/GO to crystalline TiN/rGO under microwave heating under N_2 atmosphere.(1)$2TiO_2 + 4C + N_2 \rightarrow 2TiN + 4CO\uparrow$In contrast with NH_3, N_2 was selected as the nitrogen source due to safety and cost consideration. Generally, TiN formation is difficult via gas/solid phase reactions with conventional heating methods since the strong binding of the N-N covalent is very robust [50,51]. Under microwave irradiation, however, TiN/rGO composite is easily obtained in good crystallinity and dispersion at 1200 °C in 10 min. It is widely believed that the lower initial reaction temperature and accelerated diffusion rate attributed to the dual thermal and non-thermal effects are promoted by microwave heating [52].

The sulfur content was determined by TG analysis, which was approx. 60% for rGO-S, TiO_2/rGO-S and TiN/rGO-S (Fig. 4c). All X-ray diffraction peaks are in accordance with the standard cards of pure TiN (PDF # 87–0628), TiO_2 (PDF # 73–1764) and element sulfur (PDF # 83–2283), indicating that TiN and TiO_2 are stable after sulfur incorporation (Fig. 4b). SEM images of TiN/rGO-S are shown in Fig. S5. Characterized by elemental maps, the sulfur nanoparticles have high quality dispersion on the surface of TiN/rGO composite.

To demonstrate the enhanced polysulfide adsorption ability of the as-prepared TiN/rGO-S, three samples, rGO-S, TiO_2/rGO-S and TiN/rGO-S, were respectively used as cathodes and their electrochemical properties systematically evaluated using CR2016 coin cells. The CV profiles of the first three cycles (Fig. 5a) for both TiO_2/rGO-S and TiN/rGO-S electrodes possess a similar shape. Two representative cathodic peaks at 2.19–2.41 V and 1.91–2.10 V are considered as the two stepwise reduction reactions of elemental sulfur (S_8). The high-potential cathodic peak stems from the ring open reduction of S_8 to long chain LiPSs (Li_2S_x, $4 \leq x < 8$), and the low-potential cathodic peak is known to be further reduced from LiPSs to insoluble Li_2S_2 and Li_2S [53].

Furthermore, two reduction peaks potentials upshift from TiO_2/rGO-S to TiN/rGO-S by 39–89 mV are clearly observed, indicating that the rate of electrochemical process is slower on the hybrid surface of TiO_2/rGO than TiN/rGO. The extra electron transportation process on the TiO_2/rGO interface causes additional energy loss, leading to a higher negative potential. Whereas, the oxidation peak of the TiN/rGO-S electrode (2.31 V) is lower than that of TiO_2/rGO-S (2.41 V). The obvious negative shift of the oxidation peak of TiN/rGO-S cathode implies that the TiN can enhance the rate of the oxidation process of insoluble short-chain to soluble long-chain LiPSs [54]. Meanwhile, the redox peaks of rGO-S (Fig. S6) are between the TiO_2/rGO-S and TiN/rGO-S. The substantial reduction of anodic peaks and increase in cathodic peaks of TiN/rGO-S cathode indicates that the reaction kinetics of sulfur is significantly improved in the TiN/rGO composite.

The discharging-charging profiles of the TiN/rGO-S cathode (Fig. 5b) were conducted at 0.1 C from 1st to 150th cycles. The discharging curves consist of two platforms at around 2.1 and 2.3 V, respectively. The short platform at 2.3 V corresponds to the transformation from long-chain to short-chain LiPSs, while, the flatter and longer platform at 2.1 V relates to the conversion of short-chain LiPSs to insoluble discharge products (Li_2S/Li_2S_2), which are in agreement with the CV profiles [55]. The rate capabilities of the TiN/rGO-S, TiO_2/rGO-S and rGO-S electrodes were measured by discharging-charging mode at a range of discharging rates from 0.1 to 2 C for each 10 cycles (Fig. 5c). The as-prepared TiN/rGO-S cathodes exhibit much higher capacity than those of the TiO_2/rGO-S electrodes over the entire discharging-charging process. Average reversible discharge capacities of 1143, 1020, 904, 794 and 687 mAh g^{-1} are obtained at 0.1, 0.2, 0.5, 1 and 2 C for TiN/rGO-S cathode in each 10 cycles, respectively. Notably, a stable average reversible specific capacity of 1031 mAh g^{-1} is retained once the discharging-charging rate is switched back to 0.1 C after 50 cycles under a range of different current rates, indicating well stable reversible capability [56]. In contrast, the specific capacity

of TiO_2/rGO-S electrode at 0.1, 0.2, 0.5, 1 and 2 C rates are 1028, 918, 803, 701 and 600 mAh g^{-1}, respectively. The TiO_2/rGO-S exhibits obviously lower discharge capacities than TiN/rGO-S electrode mainly due to inferior electronic conductivity, which leads to poor active material utilization ratio [57]. The capacity of the rGO-S cathodes shows a dramatic decrease with increasing current density. The average capacity of rGO-S cathode remains with only 391 mAh g^{-1} at 2 C.

In addition, the discharging and charging voltage profiles of the TiN/rGO-S cathode for the first cycle at the series current densities from 0.1 C to 2 C were measured (Fig. S7). The voltage hysteresis (ΔE) is larger at higher current rate compared to lower rate due to polarization. However, all the curves maintain two complete and flat plateaus, indicating the excellent electrochemical reaction kinetics of TiN/rGO-S composite. The cycling stability of the TiN/rGO-S, TiO_2/rGO-S and rGO-S cathodes was measured by long-term galvanostatic discharging and charging test at 0.1C. As shown in Fig. 5d, the TiN/rGO-S electrode demonstrates a high initial discharging capacity of 1197.6 mAh g^{-1}, where the reversible capacity of 888.7 mAh g^{-1} is retained after 150 cycles. By increasing the current density to 0.2C, the TiN/rGO-S electrode maintains a high initial discharging capacity of 1136 mAh g^{-1} and reversible capacity of 831 mAh g^{-1} after 200 cycles (Fig. S8), indicating good long-term cycling stability. In the case of the rGO-S electrode, the specific discharge capacity is comparable to that of TiN/rGO-S in the first cycle at 0.1 C (1216 mAh g^{-1}), but decays drastically in subsequent cycles. The low cycle stability of rGO-S is mainly due to the weak physical adsorption between rGO and LiPSs. In contrast, the TiO_2/rGO-S cathode shows a significantly lower initial discharge capacity (1070 mAh g^{-1}) due to low conductivity, but it possesses enhanced cyclic stability compared to rGO-S in the later cycles. This phenomenon can primarily be attributed to the TiO_2 nanoparticles, which can provide an extra chemical bond for the polar LiPSs [57].

Electrochemical impedance spectrum (EIS) test before cycling was conducted to investigate the internal electrochemical reaction kinetics of the three button cells. As depicted in Fig. 5e, the semicircle at high frequencies are related to the charge transfer resistance (*Rct*) at the electrolyte/electrode interface, accompanying an oblique line at the low frequency region representing the ion diffusion [58]. The *Rct* value of TiN/rGO-S cathode (31.7 Ω) is smaller than that of the rGO-S (47.3 Ω) and TiO_2/rGO-S (113.3 Ω) electrode, indicating a faster charge transfer and enhanced surface reaction between TiN and LiPSs. Fig. S9 exhibits the EIS plots of the TiN/rGO-S, TiO_2/rGO-S and rGO-S cathodes after 20 cycles at the full charged state. The high-frequency semicircles of three samples are clearly reduced compared to those of the corresponding fresh cells displayed in Fig. 5e, suggesting enhanced charge transport, rearrangement of the active material, and better electrolyte infiltration after the initial cycles. The SEM images of the cycled TiN/rGO electrode (Fig. S10) reveals that the structural integrity of the cathode remains intact.

Furthermore, high areal sulfur loading is critical to satisfy the requirement for actual application. Accordingly, the cycling performance of TiN/rGO-S electrodes with approx. 80% sulfur content and 2 mg cm^{-2} areal loading are presented in Fig. 5f. The electrodes show a high discharging capacity of 700 mAh g^{-1} at 1 C rate after the activation processes of initial three circles, and retain a reversible capacity of 460 mAh g^{-1} after 500 cycles.

To show the strong anchoring ability of the TiN/rGO for LiPSs, the equivalent total surface area of rGO, TiO_2/rGO and TiN/rGO composites were added to a solution of Li_2S_x in DOL/DEM (ratio of 1:1 by vol) and allowed to stand for 24 h. The total surface area and pore size distribution of as-added powders were determined by nitrogen adsorption/desorption isotherms measurements (Figs. S11 and S12). As shown in Fig. 6a, the mixture with TiN/rGO composite becomes colorless, implying a strong absorption between Li_2S_x and TiN. While, the TiO_2/rGO-containing solution changes color from dark brown to pale yellow. In contrast, upon

contact with rGO, the Li_2S_x solution still displays a quite conspicuous light brown color, similar to the original state.

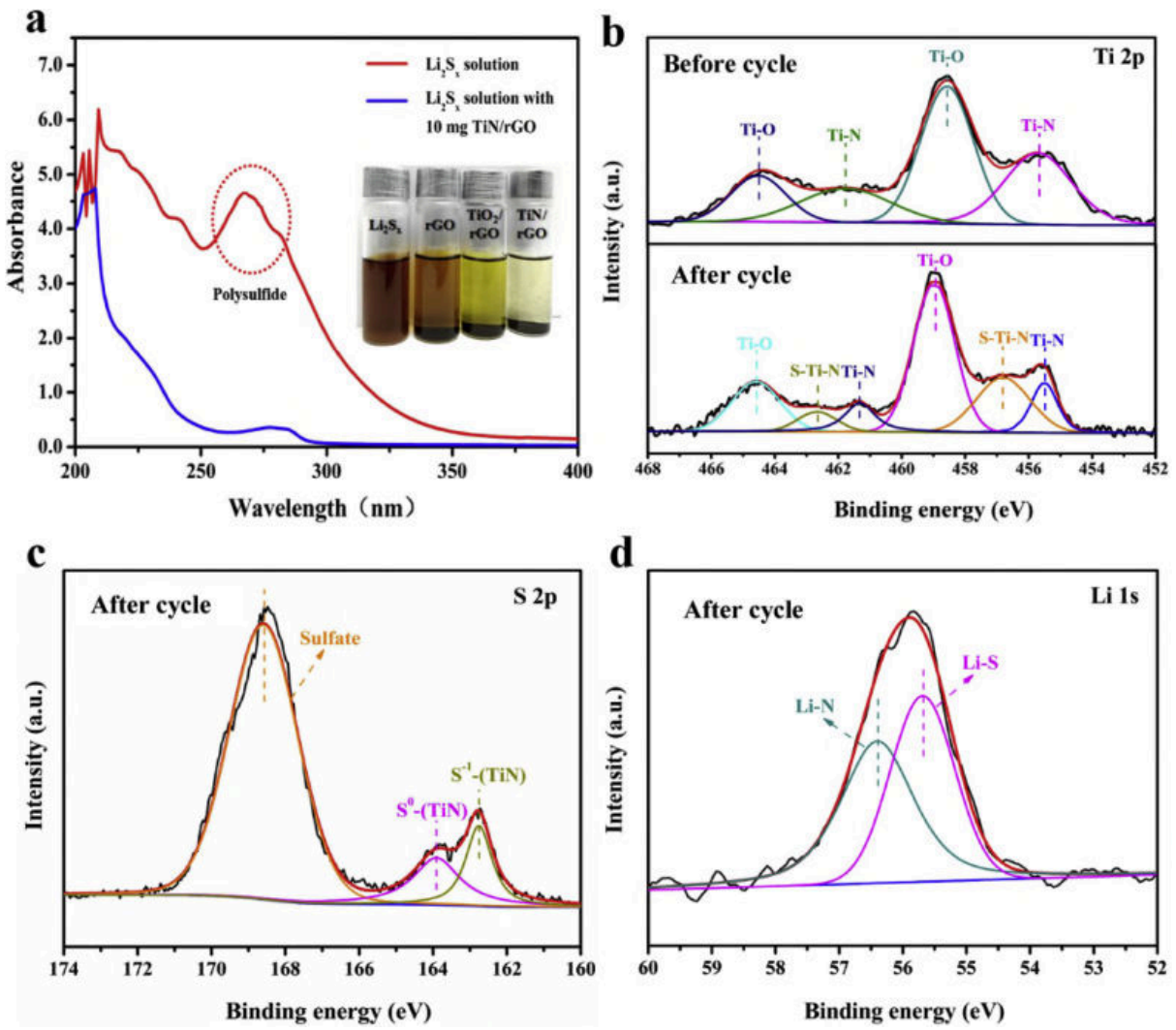


Fig. 6. (a) Ultraviolet/visible adsorption spectra of a Li_2S_x solution before and after the addition of TiN/rGO, inset image shows a photograph of a Li_2S_x solution before and after the addition of various host material; (b) XPS spectra corresponding to Ti 2P of TiN/rGO electrode before and after 100 cycles at 0.1C (1.8 V discharged state); (c) S 2P and (d) Li 1S of TiN/rGO electrode after lithiation (100 cycles at 0.1C, 1.8 V discharged state).

The ultraviolet/visible absorption test was conducted to confirm the Li_2S_x adsorption effect of TiN/rGO. The large absorption band at approx. 280 nm is attributed to the presence of S_4^{2-}/S_6^{2-} species [59]. Upon mixing with TiN/rGO, a clear decrease in peak intensity is observed, owing to the significant affinity of polysulfides toward TiN edge sites. XPS measurements were conducted to further confirm the chemical interaction between TiN/rGO and LiPSs. LiPSs is known to show a Lewis basic characteristic, while Ti atoms exposed to the rGO surface with unoccupied orbitals act as Lewis acid sites, thus, TiO_2/TiN and LiPSs can act as Lewis acid and base to contribute electrons to the Ti–S covalence, respectively. The dispersion interaction energy between TiO_2/TiN and Li_2S_4 with a value of −3.47 and −2.94 eV, is superior to the adsorption energies on known adsorbents such as C_3N_4 (−2.42 eV) and black phosphorus (Fig. S13 shows the comparison of Li_2S_4 adsorption energies of TiO_2/TiN and other absorbent materials).

The high-resolution XPS spectra corresponding to Ti 2P of TiN/rGO electrode before and after 100 cycles at 0.1C (1.8 V discharged state) are shown in Fig. 6b. Before cycling, the Ti 2p3/2 peak and Ti 2p1/2 peak of 455.6 and 461.3 eV are related to N–Ti bond for TiN [43,60]. Meanwhile, the Ti 2p3/2 peak and Ti 2p1/2 peak of 458.5 and 464.3 eV are ascribed to the Ti–O bond of oxynitride [61]. The presence of oxynitride is due to the slight oxidation passivation layer on the surface of TiN nanoparticles when exposed to the air [62]. Reports have shown that TiN thin films with low levels of oxygen content reveal a partial metallic property, indicating that the oxynitride layer on the surface of TiN nanoparticles possesses good electrical conductivity [63]. After cycling, no obvious changes in the Ti 2P peaks are observed, except for two new peaks appearing at 456.8 and 462.6 eV, which corresponds to the S–Ti–N bond, confirming the adsorption properties of TiN and LiPSs [64]. In the N 1S spectrum, before cycling, the main peaks at 397.3 and 396.5 eV are observed corresponding to TiN and oxynitride, respectively, which are consistent with the Ti 2P data (Fig. S14). Furthermore, after

100 cycles at 0.1C, an additional peak at 400.8 eV is observed, originating from the S–N–Ti bond [65]. Upon covalent bond formation the original two peaks shift toward lower binding energies owing to the similar electronegativity of sulfur and nitrogen atoms [44]. In addition, two peaks corresponding to Li–S (S^{-1}) and bridged S–S (S^0) bond are detected in the S 2p spectrum (Fig. 6c) after lithiation [66]. Similarly, a broad peak in the Li 1S spectrum of the electrode (Fig. 6d) is further divided into two peaks at 55.6 and 56.4 eV, which are related to the Li–S and Li–N bond, respectively [67]. For comparative analysis, the XPS spectra (Fig. S15) of Ti 2P of TiO_2/rGO-S electrode before and after 100 cycles at 0.1 C and S 2P of TiO_2/rGO-S electrode after lithiation were examined. This suggests that Ti–S and Li–N bonds exist between TiN nanoparticles and LiPSs endowing the TiN/rGO composite with high capacity of sulfur utilization. Moreover, recent studies have shown that TiN efficiency accelerates the decomposition of Li_2S_8, which is not observed on TiO_2 surface [67]. The electrical conductivity of TiN at room temperature is approx. 4.0×10^6 S m^{-1}, which is considerably greater that of TiO_2 ($<10^{-10}$ S m^{-1}) [68]. In combination with its strong polysulfides adsorption ability, high electrical conductivity, and acceleration mechanism to Li_2S_8, the prepared TiN/rGO based cathode enables Li–S batteries with significantly reduced potential barrier and prolonged cycling stability.

The comparison of the adsorption mechanism of rGO-S, TiO_2/rGO-S and TiN/rGO-S composites is depicted in Fig. 7. Although rGO has favorable conductivity, which facilitates the electron transfer, the liquid LiPSs can easily diffuse into the electrolyte from rGO-S cathode due to its non-polar property. Additionally, the different surface energies between rGO and deposited Li_2S nuclei increase the nucleation barrier, further increasing power wastage. On the contrary, the TiO_2/rGO-S composite possesses desirable chemical absorption toward LiPSs. Nonetheless, its poor electrical conductivity incompatible with the rGO nanosheets impedes the electron transfer between the interfaces. As for TiN/rGO-S, efficient charge transport,

strong chemisorption and electrochemical catalysis can be simultaneously satisfied, which results in enhanced electrochemical kinetics. Compared with other similar sulfur host materials summarized in Table S2, TiN/rGO can effectively improve the cyclic stability.

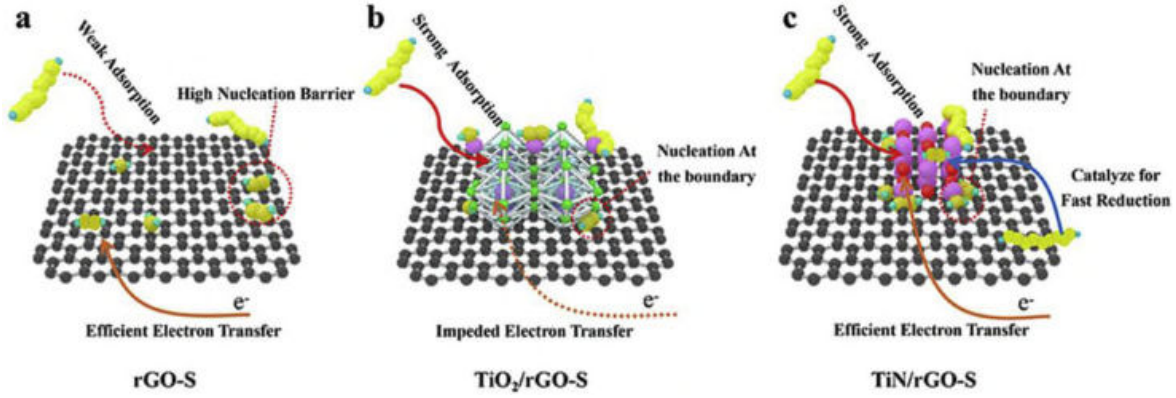


Fig. 7. Comparison of the adsorption mechanism of (a) rGO-S, (b) TiO_2/rGO-S and (c) TiN/rGO-S.

4. Conclusions

In summary, graphene-supported TiN nanoparticles hybrid was quickly synthesized by microwave reduction nitridation methods. The hybrid can serve as the sulfur host material for enhancing adsorption ability to polysulfide and reaction kinetics in Li–S batteries. We demonstrated that the TiN/rGO composites possess both a high electrical conductivity for electron transfer and polar surface for strong LiPSs/Li_2S binding. This is not the case for TiO_2/rGO and rGO. The developed TiN/rGO-S bifunctional electrode with 61.05% wt. sulfur content exhibits a high initial specific discharging capacity of 1197.6 mAh g^{-1} and retains a reversible capacity of 888.7 mAh g^{-1} after 150 cycles at 0.1 C. When the sulfur content reaches 79.62% wt., a discharging capacity of 700 mAh g^{-1} is achieved at 1 C, and capacity of 460 mAh g^{-1} is retained after 500 cycles with a capacity loss of about 0.13% per cycle. Therefore, we believe that this strategy can create an effective avenue for manufacturing other graphene

supported early-transition-metal carbonitrides not just for Li–S battery, but also potential applications in catalysis, supercapacitor, adsorption and other energy storage devices.

Author contributions section

Author 1: Jianxin Tu: Conceived and designed the study, Performed the experiments, Collected the data, Performed the analysis, Wrote the paper.

Author 2: Hejun Li: Conceived and designed the study, Reviewed and edited the manuscript.

Author 3: Tongbin Lan: Contributed data and analysis tools, Reviewed and edited the manuscript.

Author 4: Shao-Zhong Zeng: Contributed data and analysis tools, Reviewed and edited the manuscript.

Author 5: Jizhao Zou: Reviewed and edited the manuscript.

Author 6: Qi Zhang: Reviewed and edited the manuscript.

Author 7: Xierong Zeng: Conceived and designed the study. Reviewed and edited the manuscript.

Acknowledgements

The authors appreciate support by the Shenzhen Basic Research Program (No. JCYJ20170818100134570, JCYJ20160422091418366), China Postdoctoral Science Foundation (No. 2019M663054). Thanks for TEM measurement help of Instrumental Analysis Center of Shenzhen University (Xili Campus).



https://dspace.org/

Facile synthesis of TiN nanocrystals/graphene hybrid to chemically suppress the shuttle effect for lithium-sulfur batteries

Tu, Jianxin; Li, Hejun; Lan, Tongbin; Zeng, Shao-Zhong; Zou, Jizhao ...

2020-01-08
Elsevier
10.1016/j.jallcom.2020.153751
Tu J, Li H, Lan T, et al., (2020) Facile synthesis of TiN nanocrystals/graphene hybrid to chemically suppress the shuttle effect for lithium-sulfur batteries. Journal of Alloys and Compounds, Volume 822, May 2020, Article number 153751

Downloaded from a DSpace repository. https://dspace.org/